NANO LETTERS

LETTER

pubs.acs.org/NanoLett

Plasmon Enhanced Solar-to-Fuel Energy Conversion

Isabell Thomann,*,† Blaise A. Pinaud,‡ Zhebo Chen,‡ Bruce M. Clemens,† Thomas F. Jaramillo,‡ and Mark L. Brongersma*,†

†Geballe Laboratory for Advanced Materials, 476 Lomita Mall, Stanford, California 94305-4045, United States

‡Department of Chemical Engineering, 381 North-South Mall, Stanford University, Stanford, California 94305-5025, United States

Supporting Information

ABSTRACT:

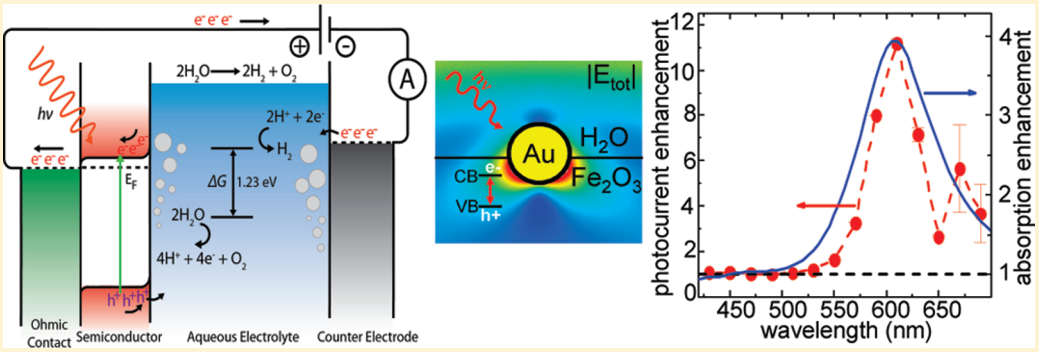

Future generations of photoelectrodes for solar fuel generation must employ inexpensive, earth-abundant absorber materials in order to provide a large-scale source of clean energy. These materials tend to have poor electrical transport properties and exhibit carrier diffusion lengths which are significantly shorter than the absorption depth of light. As a result, many photoexcited carriers are generated too far from a reactive surface and recombine instead of participating in solar-to-fuel conversion. We demonstrate that plasmonic resonances in metallic nanostructures and multilayer interference effects can be engineered to strongly concentrate sunlight close to the electrode/liquid interface, precisely where the relevant reactions take place. On comparison of spectral features in the enhanced photocurrent spectra to full-field electromagnetic simulations, the contribution of surface plasmon excitations is verified. These results open the door to the optimization of a wide variety of photochemical processes by leveraging the rapid advances in the field of plasmonics.

KEYWORDS: Plasmon, noble metal nanoparticles, iron oxide, water splitting, water oxidation, solar fuel

Solar fuel generation based on inexpensive, earth-abundant materials constitutes one potentially viable option to satisfy the demand for a terawatt scale renewable source of energy that can be stored and used on demand.[1] The efficiency of solar water splitting[2,3] based on earth-abundant materials made by using scalable processing techniques has remained low despite intensive research efforts since the 1970s. One of the underlying reasons for the observed inefficiency is that many of these materials exhibit a large mismatch between the length scales over which photon absorption takes place (up to micrometers), and the relatively short distances over which electronic carriers can be extracted (often limited to a few tens of nanometers). One possible approach to circumvent this challenge is to synthesize nanostructured electrodes in which the photon propagation and charge transport directions are orthogonalized. This type of geometry can be accomplished in wire arrays[4−6] or other nanostructures with large surface-to-volume ratios.[7] In this paper we describe how Fabry−Perot resonances in high refractive index photoelectrode materials and plasmonic resonances in metallic nanostructures can thoughtfully be engineered to enable better photon management and significant enhancements in performance. The basic concept is illustrated in Figure 1a, which shows how a metallic nanoparticle can concentrate light near a semiconductor/liquid junction to produce more photocarriers that can reach the interface and participate in the desired reactions. The concentration by the nanoparticles can further be cascaded with multilayer interference effects in the typically high refractive index photoelectrode materials.

Recently, the use of metallic nanostructures has proven extremely effective in enhancing the efficiency[8−21] of a variety of photocatalytic reactions and thin film solar cells whose performance is constrained by similar issues.[22−28] Very recently, the use of plasmon resonances in metal nanostructures has even been proposed to enhance the photoactivity of electrodes for H_2O splitting, although no net enhancements across the solar spectrum have been observed that are unambiguously attributable to plasmonic

Received: June 5, 2011
Revised: July 6, 2011
Published: July 12, 2011

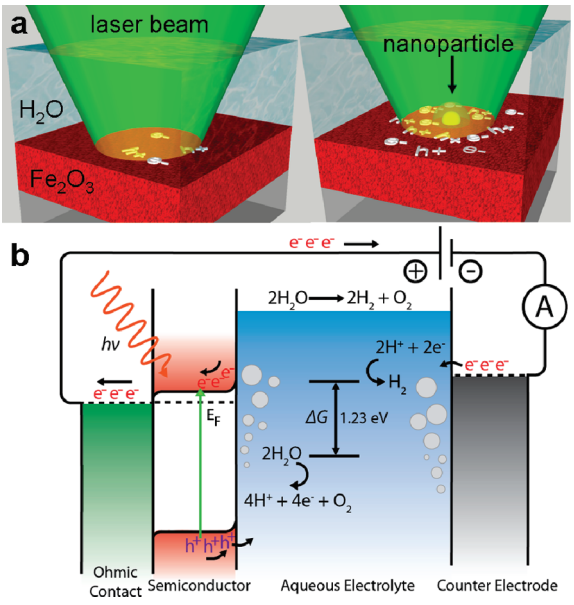

Figure 1. Beneficial effects of plasmonics on the performance of photoelectrochemical cells. (a) A schematic that illustrates how a silica coated metal nanoparticle can effectively concentrate light near the semiconductor/liquid interface. This effect increases the number of photogenerated carriers that can reach the interface and participate in desired reactions, for example, those required in water splitting to produce O_2 and H_2. (b) Schematic band diagram depicting the semiconductor absorber (left) in contact with the liquid, where the photogenerated holes drive oxygen evolution. It is this reaction that we seek to enhance using plasmonic effects with α-Fe_2O_3 as the semiconductor electrode. The generated electrons are transported to a counter electrode (right) where they can react to produce H_2 and close the circuit. Measurements of the photogenerated current as a function of the illumination wavelength can provide valuable clues on the potential importance of plasmonic effects.

effects. Metallic nanoparticles support collective electron oscillations, known as surface plasmons (SPs). At specific frequencies these charge oscillations can be driven resonantly and produce intense light fields near the metal and cause strong light scattering. As such, metal particles serve as optical antennas that operate analogously to larger radio antennas.[29] The light concentration and scattering effects were effectively harnessed to trap light inside the absorbing semiconductor layers of a solar cell and to ultimately enhance the power conversion efficiency. While absorption within the metal nanoparticles represents a possible loss mechanism in plasmon-enhanced solar photoconversion devices[25] and needs to be considered in their design, for many materials—especially ones that by themselves exhibit poor optical absorption—the beneficial effects of electromagnetic energy concentration in the semiconductor electrode can by far outweigh additional losses caused by metal absorption. The SP resonance frequency of a metal particle can be tuned across the ultraviolet, visible, and near-infrared parts of the electromagnetic spectrum through a choice of its size, shape, and dielectric environment.[30] This notion has enabled broad-band enhancements of the photocurrent across the wide solar spectrum. Rapid developments in this area were founded upon initial, convincing demonstrations that plasmonic effects are capable of boosting efficiency.[22] Key to demonstrating the importance of plasmonics in enhancing solar cell efficiency was the presence of characteristic plasmonic features in the photocurrent spectra from cells with metallic nanostructures. In this paper we aim to leverage the existing knowledge base on plasmon-enhanced photovoltaics to convincingly demonstrate that plasmonic effects can also enhance solar energy conversion to fuels.

The enhancement of solar energy conversion to fuels imposes different requirements on the plasmonic nanostructures than on solar cells. This fact can be appreciated by analyzing the materials properties of a typical photoelectrode and the band diagram of a standard photoelectrolysis cell used for water splitting. In this paper we describe a specific cell that employs iron oxide. This n-type semiconductor can be viewed as a prototypical system that is of topical interest and which shares many features with other candidate materials for future large-scale solar fuel production. Iron oxide (α-Fe_2O_3, hematite) is a material that has been extensively researched for water splitting, mainly because it is corrosion-stable, inexpensive, and earth-abundant. Its band gap is around 2.1 eV, close to an ideal value for water splitting by a single semiconductor material. One major shortcoming of iron oxide as a photoelectrode material is its poor electronic transport, with a minority carrier diffusion length on the order of 2−4 nm[31] or 20 nm.[32] In addition, Fe_2O_3 is a relatively weak absorber in the 500−600 nm range (~0.1−1 μm absorption length, far longer than the generated photocarriers can travel).

Figure 1b shows the band diagram of a cell which employs iron oxide as the photoanode. Upon illumination, photogenerated holes move toward the semiconductor/liquid interface and oxidize water to produce oxygen. The electrons generated in this oxidative process are transported through an external circuit to a metal counter electrode where they can drive hydrogen evolution. Using this circuit, we can measure the wavelength-dependent photocurrent to determine the photocurrent spectra. Driving the water splitting reaction with iron oxide requires an applied potential due to its mismatched conduction band alignment.[33] This limitation can be overcome by using the material in a tandem cell configuration with two semiconductor electrodes.[34] The band diagram suggests that issues with poor charge transport might be alleviated if metallic nanoparticles could be used to concentrate incident sunlight as close as possible to the semiconductor/liquid interface. Here, the space charge layer can quickly separate the photocarriers and deliver the holes to the Fe_2O_3/H_2O interface. For stable operation, the metallic nanoparticles will need to be chemically stable as well.

In the following, we describe a set of experiments that show (1) that metallic nanostructures can enhance the photocurrent in spectral regions near the surface plasmon resonance and (2) that the spectral dependence of the photocurrent spectra is characteristic of plasmonic structures. Our aim is to separate plasmonic effects from other chemical/physical effects that can impact the photocurrent. To this end, we show that the use of different types of metallic nanostructures and the different placement of such particles with respect to the photoelectrode material affect the photocurrent spectra in a predictable way which is consistent with plasmonic effects.

In our first experiment, we aimed to demonstrate that metal nanoparticles can enhance photocurrents while avoiding catalytic effects. To this end, we utilized Au nanoparticles coated with a nonreactive silica (SiO_2) shell. Empirically, we found the strongest photocurrent enhancements with 50 nm diameter gold particles coated with a thin silica shell. Panels b and d of Figure 2 show scanning electron microscopy images of two different Fe_2O_3 samples containing these particles. Figure 2b shows a sample with these nanoparticles deposited onto a transparent conductive

dx.doi.org/10.1021/nl201908s |*Nano Lett.* 2011, 11, 3440–3446

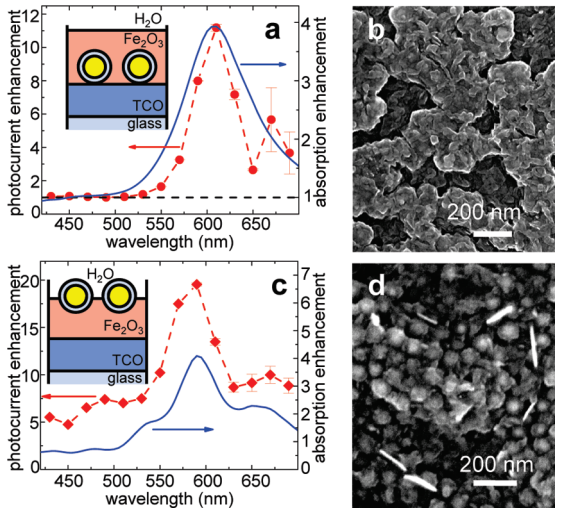

Figure 2. Photocurrent enhancement spectra for Au nanoparticles with a silica shell. (a, c) Measured photocurrent (red symbols) and simulated (solid blue lines) absorption enhancement spectra that show the beneficial effects of placing silica-coated Au particles at the bottom/on top of a 100 nm thin Fe_2O_3 photoelectrode layer. The samples are shown schematically in the insets, and in scanning electron microscopy images (b) and (d). Both samples exhibit strong (>10×) enhancement over a relatively broad wavelength range. Electromagnetic simulations (blue lines) are consistent with a plasmonic origin of the observed enhancements in the 550−650 nm wavelength range. The sample with the particles at the H_2O/Fe_2O_3 interface shows an additional, more-or-less frequency-independent enhancement (about 5−8×) that cannot be explained by electromagnetic effects but has a chemical/physical origin (see main text).

oxide electrode that was covered by a 100 nm thick iron oxide film. The presence of the nanoparticles can still be discerned underneath the thin Fe_2O_3 film. In Figure 2d identical core−shell nanoparticles were deposited on top of a 90 nm thick iron oxide film. The particles are clearly visible and are exposed to the aqueous solution during the electrochemical experiments.

Panels a and c of Figure 2 show spectral photocurrent measurements on these electrodes taken in a three-electrode photoelectrochemical cell (see Supporting Information). The photocurrent enhancement ε spectra were generated by normalizing the photocurrent $j_{NP}(\lambda)$ from a region with particles to the photocurrent $j_{ref}(\lambda)$ obtained in a region without nanoparticles, i.e., $\varepsilon(\lambda) = j_{NP}(\lambda)/j_{ref}(\lambda)$. In Figure 2a, a strong photocurrent enhancement is observed at wavelengths longer than 550 nm, whereas the photocurrent enhancement is close to unity at short wavelengths. The strongest resonant peak enhancement of 11× is observed at 610 nm. Under AM 1.5 illumination, plasmonic effects increase the wavelength-integrated photocurrent by 7% over the planar reference structure (see Figure S8 in the Supporting Information).

In panels a and c of Figure 2 we also show simulated absorption enhancement spectra obtained using full-field electromagnetic simulations (see Supporting Information). In these simulations, the absorption enhancement was determined by calculating the dissipated power in a small iron oxide region near a metal nanoparticle and near the liquid interface and taking a ratio of this dissipated power in a structure with the plasmonic nanoparticle present and in a planar reference structure. It is expected that the measured spectral photocurrent scales linearly with the dissipated power in the iron oxide probe volume. There is an excellent qualitative agreement between the simulations and the experimental results—the matching spectral shapes reveal that plasmonic effects are what give rise to improved photoactivity. An exact quantitative comparison of the power dissipation and the photocurrent is however complicated by a variety of factors. Among the most important are that typical, high-performance samples (1) possess substrate and iron oxide film roughness, (2) exhibit carrier diffusion lengths that are sample and potentially position dependent, (3) feature a nonuniformity in the nanoparticle size, shape, and density, and (4) could show positive catalytic effects[35] and enhanced charge separation or recombination caused by the introduction of metallic nanostructures[36−38] that can add to the complexity of the system. Our arguments are thus primarily based on the spectral dependence of the photocurrent enhancement, which we have found to be robust against the effects described above, enabling us to confirm the plasmonic origin of the observed enhancements.

The blue line in Figure 2a shows the simulated absorption enhancements with a single broad peak that closely resembles the spectral shape of the experimentally observed enhancements. The exact peak position is very sensitive to the dielectric environment of the metallic particle. The resonance position is controlled by the optical properties of the material surrounding the particle.[39] It is known that even nanometer scale variations in the thickness of a silica shell on a Au particle can cause observable shifts in the resonance position.[40] On the basis of the position of the nanoparticles within the Fe_2O_3 film, it is expected that the resonant wavelength of the Au particles lies between the calculated values for Au particles surrounded by SiO_2 and Au particles surrounded by Fe_2O_3. Our simulations reveal that the SP resonance of 50 nm gold particles surrounded by a thin SiO_2 shell is around 550 nm and that the resonance moves to 630 nm when this shell is replaced by Fe_2O_3 (Figure S1, Supporting Information). The experimentally observed peak falls squarely between those values. As the exact morphology and composition of the shells are unknown after the sample fabrication, we followed two approaches to mimic a mixed SiO_2/Fe_2O_3 environment in our simulations. Figure 2a shows simulation results with shells composed of a mixed SiO_2−Fe_2O_3 medium with equal amounts of each component. Similarly good agreement with the experimental results was obtained in simulations using thinner silica shells rather than mixed shells.

Figure 2c shows photocurrent enhancements for a different configuration with the silica coated Au particles deposited on top of iron oxide. For this electrode the measured photocurrent enhancement spectrum (red symbols) again displays a strong resonant peak around 590 nm, with a ∼11× peak enhancement. It also shows an almost spectrally flat region with an ∼8× enhancement. The simulation (blue line) is consistent with a plasmonic origin for the peak, but plasmonic effects cannot account for the wavelength-independent background enhancement (the electromagnetic simulation shows an enhancement close to unity at 500 nm). We speculate that this wavelength-independent enhancement in the presence of silica shells at the semiconductor/liquid interface may arise from morphological changes of the iron oxide in the presence of the nanoparticles,[41] from additional n-doping of the iron oxide surrounding the particles,[41,42] or from possible catalytic effects on water oxidation by the particles' silica shells in contact with the liquid. The additional spectral oscillations in Figure 2c compared to those in Figure 2a arise from multilayer inferences with a thicker ∼940 nm FTO (fluorine-doped tin oxide) substrate employed here, compared to the ∼150 nm ITO (tin-doped indium oxide) substrate employed in Figure 2a.

dx.doi.org/10.1021/nl201908s |*Nano Lett.* 2011, 11, 3440–3446

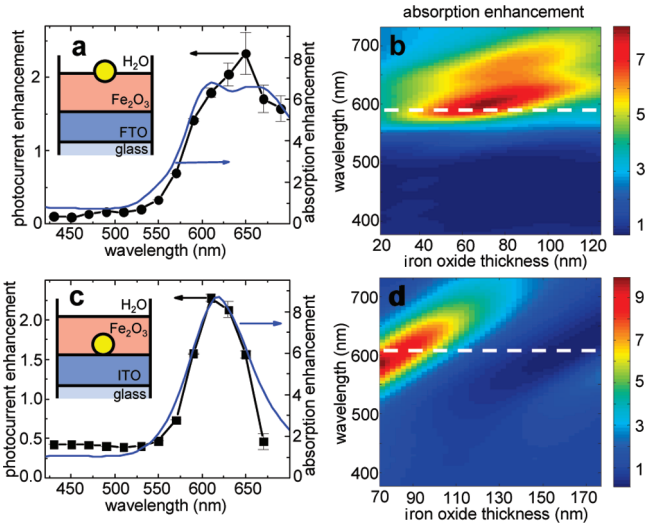

Figure 3. Plasmonic effects in the photocurrent enhancement spectra obtained with bare Au nanoparticles. (a, c) Measured photocurrent enhancement spectra (black symbols) exhibit one dominant spectral feature and are well-explained by plasmonic effects (electromagnetic simulations, blue lines). In contrast to core−shell particles, bare gold particles often show reduced photocurrents compared to simulation results, possibly due to undesired charge recombination. (b, d) Full-field electromagnetic simulations of the plasmon-enhanced absorption in a probe region near the Au particle and at the H_2O/Fe_2O_3 interface (see Figure 4a) predict strong enhancements near the surface plasmon resonance. The peak enhancement can be wavelength-tuned by varying the Fe_2O_3 thickness. This suggests that the peaks arise from an interplay between multilayer interferences and surface plasmon effects. For reference, the dashed white lines in (b) and (d) indicate the surface plasmon resonance wavelength for a 50 nm Au nanoparticle located on top of or embedded in a semi-infinite Fe_2O_3, respectively. It is important to note that the samples with Au particles on top of the Fe_2O_3 produce asymmetric photocurrent enhancement spectra, whereas the samples with particles at the bottom of the Fe_2O_3 film produce symmetric peaks. This observed behavior is a signature of plasmonic effects.

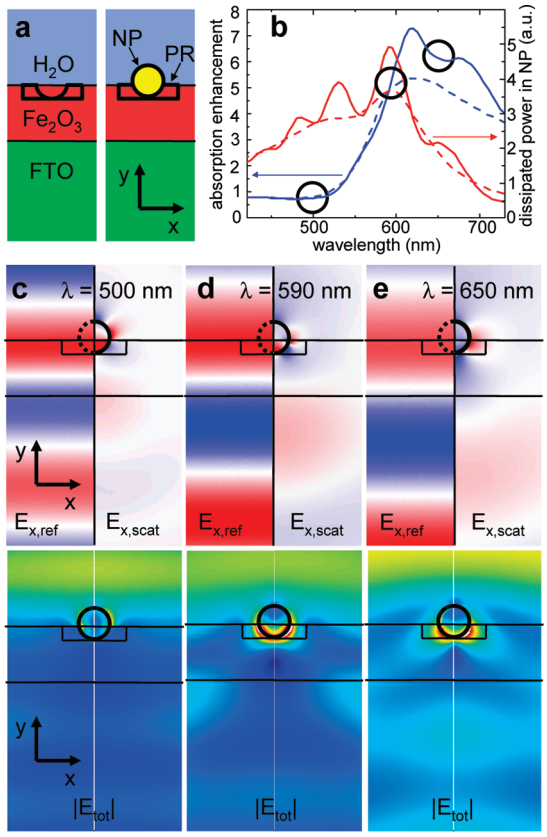

Figure 4. Full-field electromagnetic simulations explaining the physical origin of the photocurrent enhancements and their spectral distribution. (a) Simulation geometry with a Au nanoparticle (NP) on top of an Fe_2O_3 film. The probe region (PR) is the region in iron oxide in which absorption enhancements were calculated. (b) The solid lines show simulations appropriate to the multilayer geometry depicted in (a). The red line shows the absorption in the metal particle itself and the blue line shows the particle-induced absorption enhancement in the Fe_2O_3 probe region. The dashed red/blue curves show the same quantities for a semi-infinite Fe_2O_3. In these spectra the multilayer interference effects (wavelength-dependent oscillations in the photocurrent) are suppressed, and the contributions from plasmonic effects are most easily recognized. The red curves are peaked near the surface plasmon resonance wavelength of λ_{SP} = 590 nm, where incident light is most efficiently converted to heat in the particle. The blue spectrum is strongly asymmetric, which is a signature of a plasmonic effect that is explained in panels c−e. (c−e) Simulation of the *E* fields in the multilayer geometry for wavelengths of 500, 590, and 650 nm, respectively. Shown are the *x* component of the *E* field without a NP, the *x* component of the scattered field near the NP, and the modulus of the total field in the presence of the NP. For wavelengths shorter than λ_{SP}, the scattered field is out of phase with the field from the incident wave, resulting in destructive interference and low fields below the particle (c). For wavelengths longer than λ_{SP}, interference in the forward direction is constructive, resulting in an enhanced electric field (i.e., light intensity) in the probe region (e).

The measurements on the silica-coated Au particles show significant enhancements and reasonable agreement with a simple plasmonic model. The coatings on these particles give rise to several added benefits. The particles can be deposited at a high surface coverage without significant red shifts of the plasmon resonance due to particle interactions (see references 43 and 44 and Figure S2 in the Supporting Information). The high photocurrents also show that the shells are effective in preventing severe nanoparticle-induced charge recombination, which represents a well-known problem for the use of metallic nanoparticles.[38] Despite the many benefits of these coated particles, they do not serve as an ideal optical model system as their shape tends to be nonspherical, the silica shell is nondense,[45,46] and thermal processing may cause further shell deformation and interdiffusion of atomic species.[47] For this reason, we also explored the simplest possible model system which is a bare, spherical Au nanoparticle.

Figure 3 shows the measured (black symbols) photocurrent enhancement and simulated (blue lines) absorption enhancement spectra for bare, 50 nm diameter, Au particles on top (Figure 3a) and at the bottom (Figure 3c) of an iron oxide film. A comparison of the two spectra shows that the peak position and the line shape of photocurrent enhancements depend critically on the position of the nanoparticles in the iron oxide film. Particles on top of the absorber film (Figure 3a,b) produce an asymmetric line shape of the photocurrent enhancement, while particles on the bottom (Figure 3c,d) produce a more symmetric spectral feature. Both effects are true signatures of plasmonic behavior, as will be explained below. Our simulations (Figure 3b) and experiments (Figure S3, Supporting Information) show that these spectral features persist for all investigated film thicknesses. These types of spectral features have also been observed in plasmon-enhanced

dx.doi.org/10.1021/nl201908s |*Nano Lett.* 2011, 11, 3440–3446

solar cells[23] and played a critical role in proving the relevance of plasmonic effects in enhancing photovoltaics.

Panels b and d of Figure 3 show the dependence of the simulated absorption enhancements in the Fe_2O_3 with Fe_2O_3 film thickness. The plasmon resonance found in simulations of 50 nm gold particles on top of (embedded in) semi-infinite Fe_2O_3 films is indicated by the white dashed lines. For particles on top of relatively thin films, we find the maximum light concentration and absorption enhancements at slightly longer wavelengths than the particles' surface plasmon wavelength. Furthermore, the wavelength of maximum enhancement shifts linearly with the thickness of the iron oxide film. This tunability suggests that the final absorption enhancement depends on an interplay between plasmonic and multilayer interference effects, as opposed to being simply determined by the spectral location of the particle's surface plasmon resonance, as is commonly assumed.

The mechanism by which plasmonic resonances allow one to control the flow of electromagnetic energy into the absorber can be understood from plots of the electric field distributions in our structures. Figure 4a shows two simulation geometries consisting of a planar reference structure (left) and the same structure with a Au nanoparticle placed on top of the Fe_2O_3. This configuration results in the asymmetric photocurrent spectrum. The probe region (PR) in iron oxide in which absorption enhancements were calculated is indicated in black. In Figure 4b the simulated absorption enhancements in the probe regions are shown together with the dissipated power in the nanoparticle. The spectra are complicated by multilayer interference effects that produce oscillations in the spectra in addition to the strong plasmonic resonance peaks (see the dashed line in Figure 4b for a comparison to the plasmonic peak shape of a semi-infinite iron oxide film). The results in Figure 4b clearly demonstrate that the interplay between plasmon resonance and multilayer interferences can be optimized, enabling additional spectral tuning and larger enhancements compared to semi-infinite films or unoptimized multilayer structures (see Figure 3b,d).

The simulated electric field distributions generated by bare Au nanoparticles on top of iron oxide can explain the asymmetric line shape versus wavelength. We will show that it results from the interference between the incident light wave and the scattered fields from the particle. Panels c−e of Figure 4 show these distributions for wavelengths of 500 nm (shorter than the plasmon resonance wavelength, $\lambda < \lambda_{SP}$), 590 nm ($\lambda = \lambda_{SP}$), and 650 nm ($\lambda > \lambda_{SP}$), respectively. We plot the x component of the electric field without the nanoparticle present, the x component of the scattered- and near-field of the nanoparticle, and the modulus of the total field in the presence of the nanoparticle. At wavelengths shorter than the SP resonance wavelength, the electron oscillations in the metal particle can no longer follow the rapid field variations of the incident light wave and the scattered fields pick up a significant phase shift. This leads to a destructive interference between the incident light and the scattered light in the forward direction (i.e., below the particle and in the probe region in Figure 4c). This resulting lower light intensity is the cause of a lower photocurrent at wavelengths where $\lambda < \lambda_{SP}$. In contrast, Figure 4e shows that at longer wavelengths ($\lambda > \lambda_{SP}$), the interference in the forward direction is constructive, effectively increasing the light intensity in the probe region in the absorber film and enhancing the photocurrent. We note that interference effects also govern the observed enhancements for Au particles placed at the bottom of an Fe_2O_3 film (Figure 3c,d). Here constructive interference in the backward direction enables strong enhancements at wavelengths shorter than the SP resonance (500−600 nm region for the thinnest films in Figure 3d). These data not only highlight the importance of plasmonic effects in the generated photocurrent but also provide practical considerations for the design of future plasmon-enhanced photoelectrodes.

We have shown that plasmonic structures can circumvent the traditional compromise between photon absorption and carrier extraction in photoelectrodes made from inexpensive, earth-abundant semiconductor materials. Future efforts should be aimed at designing plasmonic enhancement structures that are effective at shorter wavelengths. Gold is limited in this respect, as its plasmon resonance is around 530 nm or longer, depending on the host medium. Metals with plasmon resonances in the near-UV, such as aluminum or silver, can be tuned into the region of interest by choice of size, shape, dielectric environment, and multilayer interference effects. Such metals need to be protected against corrosion, e.g., by covering them with inert shells, and we hope that our work will stimulate further materials research efforts in this direction.

We anticipate that the concepts described here will also be highly relevant to the development of future, more efficient multijunction photoelectrochemical cells, where sunlight is split into multiple spectral components, each of which requires its own optical tailoring and enhancement strategies. Finally, it is worth noting that plasmon-enhanced photon management will be of value to other high-impact photocatalysis applications, including the removal of toxic compounds from the environment and large-scale water purification.[48]

■ ASSOCIATED CONTENT

Supporting Information. Detailed experimental procedures, additional information regarding the electromagnetic simulations, additional data supporting the conclusions of the main text, further details on the photoelectrochemical characterization of iron oxide electrodes, and materials characterization of the iron oxide photoelectrodes. This material is available free of charge via the Internet at http://pubs.acs.org

■ AUTHOR INFORMATION

Corresponding Author
*E-mail: ithomann@stanford.edu; brongersma@stanford.edu.

■ ACKNOWLEDGMENT

We acknowledge fruitful collaborations and discussions with Stacey Bent's and Bruce Clemens' groups and thank Jonathan Bakke for ALD work. We gratefully acknowledge Wenshan Cai for help with simulations and Tom Carver for e-beam evaporations. This work was supported by the Center on Nanostructuring for Efficient Energy Conversion (CNEEC) at Stanford University, an Energy Frontier Research Center funded by the U.S. Department of Energy, Office of Science, Office of Basic Energy Sciences under Award Number DE-SC0001060. I. Thomann and M. L. Brongersma also acknowledge support from Samsung. I. Thomann gratefully acknowledges a postdoctoral fellowship from the Deutsche Forschungsgemeinschaft (DFG). B. Pinaud gratefully acknowledges a graduate fellowship from the Natural Sciences and Engineering Research Council of Canada.

REFERENCES

(1) Lewis, N. S.; Nocera, D. G. Powering the planet: Chemical challenges in solar energy utilization. *Proc. Natl. Acad. Sci. U.S.A.* **2006**, *103*, 15729–15735.

(2) Chen, X.; Shen, S.; Guo, L.; Mao, S. S. Semiconductor-based Photocatalytic Hydrogen Generation. *Chem. Rev.* **2010**, *110*, 6503.

(3) Zou, Z.; Ye, J.; Sayama, K.; Arakawa, H. Direct splitting of water under visible light irradiation with an oxide semiconductor photocatalyst. *Nature* **2001**, *414*, 625.

(4) Boettcher, S. W.; Spurgeon, J. M.; Putnam, M. C.; Warren, E. L.; Turner-Evans, D. B.; Kelzenberg, M. D.; Maiolo, J. R.; Atwater, H. A.; Lewis, N. S. Energy-Conversion Properties of Vapor-Liquid-Solid-Grown Silicon Wire-Array Photocathodes. *Science* **2010**, *327*, 185.

(5) Beermann, N.; Vayssieres, L.; Lindquist, S. E.; Hagfeldt, A. Photoelectrochemical studies of oriented nanorod thin films of hematite. *J. Electrochem. Soc.* **2000**, *147*, 2456–2461.

(6) Goodey, A. P.; Eichfeld, S. M.; Lew, K.-K.; Redwing, J. M.; Mallouk, T. E. Silicon Nanowire Array Photoelectrochemical Cells. *J. Am. Chem. Soc.* **2007**, *129*, 12344–12345.

(7) Kay, A.; Cesar, I.; Grätzel, M. New Benchmark for Water Photooxidation by Nanostructured α-Fe_2O_3 Films. *J. Am. Chem. Soc.* **2006**, *128*, 15714–15721.

(8) Awazu, K.; Fujimake, M.; Rockstuhl, C.; Tominaga, J.; Murakami, H.; Ohki, Y.; Yoshida, N.; Watanabe, T. A plasmonic photocatalyst consisting of silver nanoparticles embedded in titanium dioxide. *J. Am. Chem. Soc.* **2008**, *130*, 1676.

(9) Kowalska, E., Abe, R., Ohtani, B. Visible light-induced photocatalytic reaction of gold-modified titainium(IV) oxide particles: action spectrum analysis. *Chem. Commun. 241* (**2009**).

(10) Hägglund, C.; Apell, S. P. Resource efficient plasmon-based 2D-photovoltaics with reflective support. *Opt. Express* **2010**, *18*, A343.

(11) Hägglund, C.; Apell, S. P.; Kasemo, B. Maximized Optical Absorption in Ultrathin Films and Its Application to Plasmon-Based Two-Dimensional Photovoltaics. *Nano Lett.* **2011**, *11*, 915.

(12) Christopher, P.; Ingram, D. B.; Linic, S. Enhancing photochemical activity of semiconductor nanoparticles with optically active Ag nanostructures: Photochemistry mediated by Ag surface plasmons. *J. Phys. Chem. C* **2010**, *114*, 9173.

(13) Mori, K.; Kawashima, M.; Che, M.; Yamashita, H. Enhancement of the Photoinduced Oxidation Activity of a Ruthenium(II) Complex Anchored on Silica-Coated Silver Nanoparticles by Localized Surface Plasmon Resonance. *Angew. Chem., Int. Ed.* **2010**, *49*, 8598.

(14) Zhou, X.; Hu, C.; Hu, X.; Peng, T.; Qu, J. Plasmon-Assisted Degradation of Toxic Pollutants with Ag-AgBr/Al2O3 under Visible-Light Irradiation. *J. Phys. Chem. C* **2010**, *114*, 2746.

(15) Neatu, S.; Cojocaru, B.; Parvulescu, V. I.; Somoghi, V.; Alvaro, M.; Garcia, H. . Visible-light C-heteroatom bond cleavage and detoxification of chemical warfare agents using titania-supported gold nanoparticles as photocatalyst. *J. Mater. Chem.* **2010**, *20*, 4050.

(16) Tian, Y.; Tatsuma, T. Mechanisms and Applications of Plasmon-Induced Charge Separation at TiO2 Films Loaded with Gold Nanoparticles. *J. Am. Chem. Soc.* **2005**, *127*, 7632.

(17) Chen, J.-J.; Wu, J. C. S.; Wu, P. C.; Tsai, D. P. Plasmonic Photocatalyst for H2 Evolution in Photocatalytic Water Splitting. *J. Phys. Chem. C* **2011**, *115*, 210.

(18) Zhai, W.; Xue, S.; Zhu, A.; Luo, Y.; Tian, Y. Plasmon-Driven Selective Oxidation of Aromatic Alcohols to Aldehydes in Water with Recyclable Pt/TiO_2 Nanocomposites. *ChemCatChem* **2011**, *3*, 127.

(19) Silva, C. G.; Juarez, R.; Marino, T.; Molinari, R.; Garcia, H. Influence of Excitation Wavelength (UV or Visible Light) on the Photocatalytic Activity of Titania Containing Gold Nanoparticles for the Generation of Hydrogen or Oxygen from Water. *J. Am. Chem. Soc.* **2011**, *133*, 595.

(20) Lui, Z.; Hou, W.; Pavaskar, P.; Aykol, M.; Cronin, S. B. Plasmon Resonant Enhancement of Photocatalytic Water Splitting Under Visible Illumination. *Nano Lett.* **2011**, *11*, 1111.

(21) Solarska, R.; Krolikowska, A.; Augustynski, J. Silver Nanoparticle Induced Photocurrent Enhancement at WO3 Photoanodes. *Angew. Chem., Int. Ed.* **2010**, *49*, 7980.

(22) Atwater, H. A.; Polman, A. Plasmonics for improved photovoltaic devices. *Nat. Mater.* **2010**, *9*, 205.

(23) Yu, E. T. In *Nanotechnology for Photovoltaics*; Tsakalakos, L., Ed.; CRC Press: Boca Raton, FL2010.

(24) Pillai, S.; Catchpole, K. R.; Trupke, T.; Green, M. A. Surface plasmon enhanced silicon solar cells. *J. Appl. Phys.* **2007**, *101*, 093105.

(25) Pala, R. A.; White, J.; Barnard, E.; Liu, J.; Brongersma, M. L. Design of Plasmonic Thin-Film Solar Cells with Broadband Absorption Enhancements. *Adv. Mater.* **2009**, *21*, 1–6.

(26) Hägglund, C.; Zäch, M.; Kasemo, B. Enhanced charge carrier generation in dye sensitized solar cells by nanoparticle plasmons. *Appl. Phys. Lett.* **2008**, *92*, 013113.

(27) Fahr, S.; Rockstuhl, C.; Lederer, F. Metallic nanoparticles as intermediate reflectors in tandem solar cells. *Appl. Phys. Lett.* **2009**, *95*, 121105.

(28) Ding, I.-K.; Zhu, J.; Cai, W.; Moon, S.-J.; Cai, N.; Wang, P.; Zakeeruddin, S. M.; Grätzel, M.; Brongersma, M. L.; Cui, Y.; McGehee, M. D. Plasmonic Dye-Sensitized Solar Cells. *Adv. Energy Mater.* **2011**, *1*, 52–57.

(29) Bharadwaj, P.; Deutsch, B.; Novotny, L. Optical Antennas. *Adv. Opt. Photonics* **2009**, *1*, 438.

(30) Schuller, J. A.; Barnard, E. S.; Cai, W.; Jun, Y. C.; White, J. S.; Brongersma, M.L. . Plasmonics for extreme light concentration and manipulation. *Nat. Mater.* **2010**, *9*, 193–204.

(31) Kennedy, J. H.; Frese, K. W. Photooxidation of Water at α-Fe_2O_3 Electrodes. *J. Electrochem. Soc.* **1978**, *125*, 709.

(32) Dare-Edwards, M. P.; Goodenough, J. B.; Hamnett, A.; Trevellick, P. R. Electrochemistry and photoelectrochemistry of iron(III) oxide. *J. Chem. Soc., Faraday Trans. 1* **1983**, *79*, 2027.

(33) Grätzel, M. Photoelectrochemical cells. *Nature* **2001**, *338*, 414.

(34) Miller, E. L.; Rocheleau, R. E.; Khan, S. A hybrid multijunction photoelectrode for hydrogen production fabricated with amorphous silicon/germanium and iron oxide thin films. *Int. J. Hydrogen Energy* **2004**, *29*, 907–914.

(35) Mavrikakis, M.; Stoltze, P.; Nørskov, J. K. Making gold less noble. *Catal. Lett.* **2000**, *64*, 101–106.

(36) Subramanian, V.; Wolf, E.; Kamat, P. V. Semiconductor-Metal Composite Nanostructures. To What Extent Do Metal Nanoparticles Improve the Photocatalytic Activity of TiO2 Films?. *J. Phys. Chem. B* **2001**, *105*, 11439–11446.

(37) Watanabe, A.; Kozuka, H. Photoanodic Properties of Sol-Gel-Derived Fe2O3 Thin Films Containing Dispersed Gold and Silver Particles. *J. Phys. Chem. B* **2003**, *107*, 12713–12720.

(38) Thimsen, E.; Le Formal, F.; Grätzel, M.; Warren, S. C. Influence of Plasmonic Au Nanoparticles on the Photoactivity of Fe_2O_3 Electrodes for Water Splitting. *Nano Lett.* **2011**, *11*, 35–43.

(39) Kelly, K. L.; Coronado, E.; Zhao, L. L; Schatz, G. C. The Optical Properties of Metal Nanoparticles: The Influence of Size, Shape, and Dielectric Environment. *J. Phys. Chem. B* **2003**, *107*, 668.

(40) Ung, T.; Liz-Marzan, L. M.; Mulvaney, P. Gold nanoparticle thin films. *Colloids Surf., A* **2002**, *202*, 119–126.

(41) Cesar, I.; Kay, A.; Gonzalez Martinez, J. A.; Grätzel, M. Translucent Thin Film Fe_2O_3 Photoanodes for Efficient Water Splitting by Sunlight: Nanostructure-Directing Effect of Si-Doping. *J. Am. Chem. Soc.* **2006**, *128*, 4582–4583.

(42) Liang, Y., Enache, C. S., van de Krol, R. Photoelectrochemical Characterization of Sprayed α-Fe2O3 Thin Films: Influence of Si Doping and SnO2 Interfacial Layer. *Int. J. Photoenergy* **2008**, doi:10.1155/2008/739864.

(43) Jensen, T. R.; Schatz, G. C.; Van Duyne, R. P. Nanosphere Lithography: Surface Plasmon Resonance Spectrum of a Periodic Array of Silver Nanoparticles by Ultraviolet-Visible Extinction Spectroscopy and Electrodynamic Modeling. *J. Phys. Chem. B* **1999**, *103*, 2394–2401.

(44) Liu, Z.; Wang, H.; Li, H. Red shift of plasmon resonance frequency due to the interacting Ag nanoparticles embedded in single crystal SiO_2 by implantation. *Appl. Phys. Lett.* **1998**, *72*, 1823.

(45) Gautier, C.; Cunningham, A.; Si-Ahmed, L.; Robert, G.; Bürgi, T. Pigments based on silica-coated gold nanorods: Synthesis, colouring strength, functionalisation, extrusion, thermal stability and colour evolution. *Gold Bull.* **2010**, *43*, 94.

(46) Zhang, K.; Wang, W.; Cheng, W.; Xing, X.; Mo, G.; Cai, Q.; Chen, Z.; Wu, Z. Temperature-Induced Interfacial Change in Au@SiO2 Core-Shell Nanoparticles Detected by Extended X-ray Absorption Fine Structure. *J. Phys. Chem. C* **2010**, *114*, 41.

(47) Forman, A. J.; Park, J.-N.; Tang, W.; Hu, Y.-S.; Stucky, G. D.; McFarland, E. W. Silica-Encapsulated Pd Nanoparticles as a Regenerable and Sintering-Resistant Catalyst. *ChemCatChem* **2010**, *2*, 1318–1324.

(48) Kwon, S.; Fan, M.; Cooper, A. T.; Yang, H. Photocatalytic Applications of Micro- and Nano-TiO_2 in Environmental Engineering. *Crit. Rev. Environ. Sci. Technol.* **2008**, *38*, 197–226.